# Design and Implementation of a Hardware Test-bed for Real-time EV-Grid Integration Analysis

Emin Ucer

Center for Integrated Mobility Sciences National Renewable Energy Laboratory Golden, Colorado emin.ucer@nrel.gov Mithat J. Kisacikoglu

Center for Integrated Mobility Sciences

National Renewable Energy Laboratory

Golden, Colorado

john.kisacikoglu@nrel.gov

Abstract—This study presents the design of an electric vehicle (EV)-grid integration hardware test-bed to implement smart EV charging algorithms. The proposed test-bed allows for creating various grid events via flexible integration of power hardware (e.g., controllable loads, and battery energy storage systems) and analyzing their impacts on EV charging. The design uses a realtime digital simulator (OPAL-RT OP5600) to simulate a complex distribution grid model with primary and secondary networks. A grid simulator (AMETEK MX22.5) physically realizes a selected node of the simulated grid to power actual loads, including a Nissan Leaf EV and a load bank. The EVGI test-bed is demonstrated based on the custom hardware and software implementation of the J1772 charging protocol using dSPACE MicroLabBox. We tested the proposed hardware test-bed by implementing a machine learning (ML) supported and decentralized EV charging algorithm based on the Additive Increase and Multiplicative Decrease (AIMD) control method. The results showed that the EV charging current successfully followed the control commands generated by the proposed smart charging controller running on the EVSE and regulated the charging power to effectively reduce the system loading caused by high EV penetration.

Index Terms—EV-Grid integration, hardware test-bed, real-time simulation

### I. INTRODUCTION

As electric vehicles (EVs) become more wide-spread, their possible adverse impacts on electric power distribution grids have been a major concern. High penetration of EVs with uncontrolled charging could easily put such a critical infrastructure in a great danger, effecting many operations, businesses, and productions at high costs. Mass EV-grid integration (EVGI) increases the peak loading of the grid. Furthermore, it can even overload the capacity of the system transformers and distribution lines causing thermal overheating, faster ageing, and even failure of equipment at high penetration levels [1], [2]. These impacts could be observed mainly on the network voltage in the form of severe voltage drops, and even blackouts [3]–[7]. As an example, the service interruptions due to severe cold weather occurred in Texas in February 2021 showed that the grid could easily lose its balance if fast actions are not taken to respond to increased demand or loss of generation

Most of this work was completed when the authors were affiliated with the University of Alabama, Tuscaloosa, AL.

This material is based upon work supported by the National Science Foundation under Award No 1755996.

capacity [8]–[10]. Mass transition to electrified transportation will make this situation harder to cope with. Therefore, every stage of EVGI has to be carefully analyzed, planned, designed, and implemented. It starts from preserving high level power grid stability and resiliency down to satisfying customer-end expectations, benefits, and quality of service.

One important stage of this integration is designing smart charging management algorithms and testing them on EVs with the aid of real-time simulators (RTS) to evaluate their performance and impacts before the final implementation in the field. This stage utilizes the prototyping process and helps foresee possible shortcomings and design flaws, and even failures of the tested algorithms, hence saves money, time, and effort. This is also useful to see whether fairly abstracted and complex charging algorithms can be implemented on real EVs. A real-time emulated EVGI test-bed allows us to fully analyze charging EV and other load dynamics under a wide range of situations in a non-destructive environment [11]. It also provides an opportunity to test the developed algorithms using the available communication standards between EV supply equipment (EVSE) and EV. Therefore, this work presents a new hardware test-bed design that is intended to be used mainly for EVGI testing.

The proposed hardware-in-the-loop (HIL) test-beds in [12], [13] only utilize real-time simulators to emulate the EV and grid, and no power hardware is involved. The grid model complexity is also low since they used a microgrid model of a workplace. The authors in [14] features a slightly more complex grid model but only investigates the primary network, reducing the fidelity of the model. There is also no power hardware, and all tests are performed by HIL simulators. A power HIL test-bed is proposed in [15], but the simulated grid-side modeling only consists of a voltage source and grid impedance, implying a low-fidelity model. A similar work is proposed in [16], but it suffers from the poor grid modeling and lack of real-time simulation. Authors in [17] propose an EV test-bed, but it lacks the grid modeling and simulation side of the problem, and uses only Lithium-ion batteries and chargers to emulate EV charging.

Our work differs from the existing literature as follows: (1) We propose a power HIL design that employs both realtime simulation and power hardware integration; (2) we use a complex distribution system, modeling both primary and secondary sides up to 80 end-nodes that have real power consumption profiles; (3) we demonstrate the integration of a real EV using the available communication interface and show how smart charging algorithms can be implemented via the standard communication on a custom-designed EVSE; (4) we give a complete guideline at the component level on how to design such an integrated test-bed; and (5) we demonstrate the implementation of a smart charging control algorithm on the EV using the proposed HIL test-bed.

### II. HARDWARE TEST-BED DESIGN

The overview of the designed EVGI test-bed is shown in Fig. 1. The test-bed involves the following components: RTS (OPAL-RT OP5600), grid simulator (Ametek MX22.5), hardware and software implementation of a custom EVSE solution, 2019 Nissan Leaf EV, resistive load bank for residential load emulation, and energy storage system emulation using Typhoon HIL 402 device. In this work, we only demonstrated the EV charging operation, but the test-bed has the capability of integrating and testing a virtual converter for a controller-HIL operation, which is also investigated in a separate work of the authors [18].

A detailed power distribution grid model with primary and secondary networks is developed and simulated on the RTS. The RTS generates real-time voltage reference signals for all end-nodes. One secondary end-node in the test distribution grid is physically realized by feeding its voltage reference signal to the grid simulator. The output of the grid simulator supplies power to EV. EV is charged using a custom EVSE, which monitors the node voltage and controls the charging current via implementing a distributed charging control algorithm. The role, design specifications, and operation of each EVGI hardware component are described next.

#### A. Real Time Simulator (RTS)

The RTS is one of the core components of the test-bed. The chosen RTS should ensure the targeted performance criterion required by application constraints at a reasonable cost. In this design, a multi-core processor based target platform OPAL-RT OP5600 is used for real-time execution of the developed distribution grid model. This platform features 12 Intel processor cores clocking at 3.4 GHz that can be operated in parallel, and includes a SPARTAN-3 FPGA card for the I/O interface with 256 analog and digital I/O lines.

RTS performance is often evaluated based on computation time for a given accuracy level, which in our case is the simulation resolution (i.e., step time). As the simulated model gets more complicated and grows in scale, the required computation resources and time increase causing overruns and inaccurate solutions. In the case of real-time simulation of a distribution grid, the simulation step time  $(T_{step})$  has to be considerably smaller than the grid voltage period  $(T_{grid})$ , i.e.,  $T_{step} \ll T_{grid} = 1/60 \, \mathrm{Hz} \approx 17 \, \mathrm{ms}$ . Most RTS platforms have maximum step times in the range of microseconds  $(\mu s)$ 

that will be sufficient to capture dynamics of an EVGI testbed, which can be operated in the millisecond range. We used  $T_{step} = 250 \mu s$  for our simulations that would generate 4000 solutions/samples per second. This also sets the sampling frequency for any input/output data accusation and feedback channel.

To realize one end-node, the voltage of the end-node is scaled and transferred from one of the ANALOG-OUT channels of OP5600 to the grid simulator. This end-node is turned into an actual, physical node to which the EV and other loads are connected. This connection is completed by feeding the resulting EV current measurement back to the model running on the RTS through its ANALOG-IN channels, forming an HIL environment. This feedback closes the loop ensuring that the hardware power consumption is accurately simulated in the digital environment. Due to the computational limitations of OPAL-RT, a moderate test distribution grid with its primary and secondary networks is modeled to run in real-time as shown in Fig. 1. Secondary network modeling is necessary from a practical standpoint as most Level-2 charging takes place at residential locations. EV charging dynamics also have significant impacts on the local service voltage; thus, the secondary network modeling helps us see this impact on the operation of charging controllers.

The grid model has five neighborhoods modeled as primary nodes. These neighborhoods are shown as red and green circles in Fig. 1, and each has 16 inner nodes representing residential houses. Each house is modeled as a secondary end-node, and a group of four houses are powered by a  $25\,\mathrm{kVA}$  service transformer [19]. The primary node voltage of the service transformer is common to the houses connected to the same transformer. Overall, the grid consists of  $5\times16=80$  end-nodes. Each end-node has a unique load profile collected using eGauge smart meter [20]–[22]. There are also two commercial office loads connected to the blue and green nodes in Fig. 1. The developed grid model is run in a single core of OPAL-RT.

In the case of high model complexity, the model can be decoupled and split into sub-models operating in parallel in different processor cores. Since the distribution grid lines are usually much shorter than transmission lines, the propagation delay between the decoupled subsystems must also be very small to solve the system accurately. However, this delay is usually much smaller than the minimum step time ( $\approx 10~\mu s$ ) of many real-time simulators causing computational overruns and inaccuracies. This was one of the major challenges preventing us from developing larger and more complex distribution grid models. Some compensated line models are also proposed to work around this problem [23], [24], but they were not incorporated in this study.

Other important challenges are the simulation duration and discharging EV batteries. Long simulation times (more than three hours) can be overwhelming for the experiment operator and increase the risk of danger. Additionally, driving the EV to discharge its battery after every long test could be very

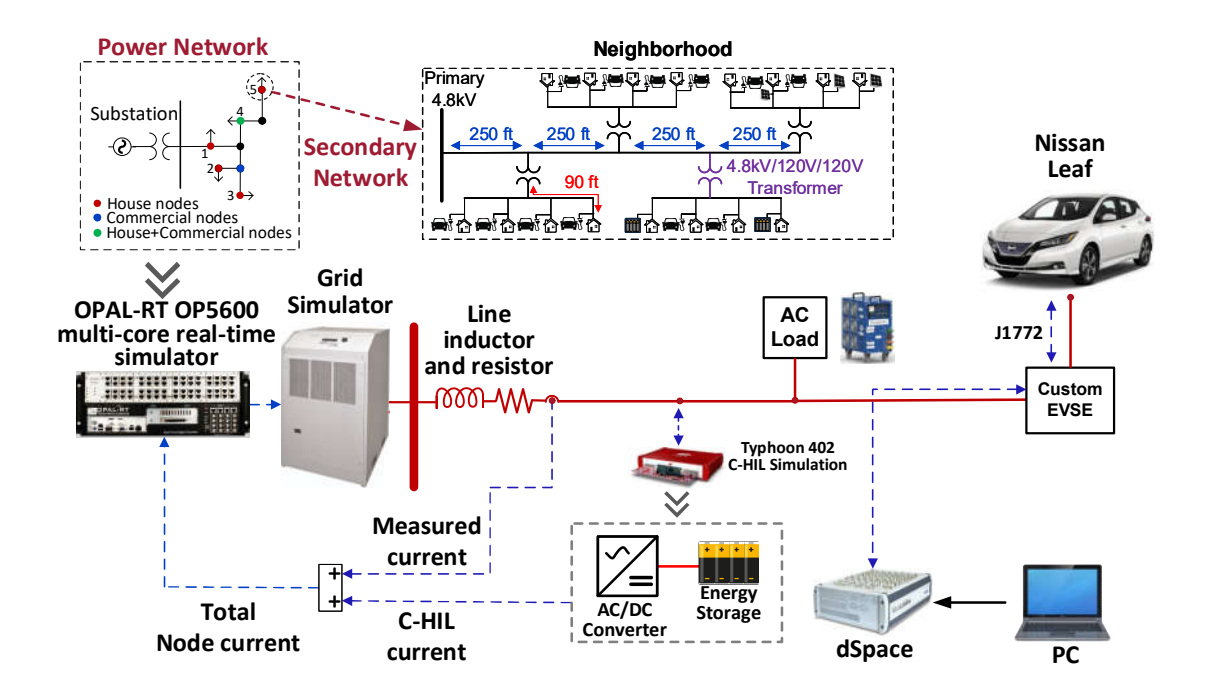


Fig. 1. Overview of the designed EVGI test-bed.

time consuming and cumbersome  $^{1}$ . For these reasons, the hardware simulations are performed for the first one hour of the simulation peak times (05:30 PM-6:30 PM). The EV arrival times are adjusted based on a mean and standard deviation of 05:30 PM and 1 min, respectively. This grid operates around the peak power of 442 kVA with no EV penetration. When EVs (of Nissan Leaf type) are fully integrated at the rated charging power and with a 40 mi of equivalent energy demand, the peak power goes up to 960 kVA. The physically realized end-node for the HIL operation is located in the  $5^{th}$  neighborhood shown in a circle in Fig. 1.

### B. Grid Simulator

The voltage reference signal generated by the RTS must be amplified up to the nominal voltage level of the simulated end-nodes, i.e.,  $240\,\mathrm{Vrms}$ . For this purpose, a programmable grid simulator is used. Our test-bed features an AMETEK MX22.5 rated at  $22.5\,\mathrm{kVA}$ . It has a three-phase AC input and provides both programmable three-phase and single-phase AC, and DC outputs. When set to the voltage control mode, the grid simulator accepts a voltage reference signal between  $0-7\,\mathrm{Vrms}$  and adjust its output voltage based on this input. The grid simulator output is connected to the end-node loads through a line impedance consisting of a  $150\,\mathrm{mH}$  inductor and a  $0.1\Omega$ ,  $250\,\mathrm{W}$  power resistor emulating the impedance of an underground service cable as shown in Fig. 1.

### C. Hardware and Software Implementation of EVSE

One must establish a standard charging standard to interface the EV with the grid to administer the charging process. The standard for Level-2 charging in North America that an EVSE must implement is SAE J1772 [25]. The protocol dictates a low level communication between EVSE and EV. The communication signal is called control pilot (CP), and it is a  $1\,\mathrm{kHz}$  square wave with its low held at  $-12\mathrm{V}$  and its high varying through different voltage levels (e.g.,  $12\mathrm{V}$ ,  $9\mathrm{V}$ ,  $6\mathrm{V}$ , and  $3\mathrm{V}$ ) corresponding to different EV states. These states are described in Table I.

The duty cycle of the CP determines the maximum charging current of EV, thus allows us to control the charging current based on the charging control algorithm. The relationship between the duty cycle of the CP and the charging current is given by (1):

$$I_c = \begin{cases} 0.6 \times \text{Duty cycle} & \text{if } 6A \le I_c < 51A \\ (\text{Duty cycle} - 64) \times 2.5 & \text{if } 51A \le I_c \le 80A \end{cases} \tag{1}$$

To implement the EVSE, a dSpace MicroLabBox (MLBX) has been utilized. The CP is generated by a dedicated PWM module of MLBX for a given frequency (1 kHz) and duty cycle. An additional auxiliary EVSE circuit was designed to shift and scale the generated PWM signal from 0-5V to the desired +/-12V level. The CP signal changes its high value

TABLE I J1772 PILOT SIGNAL STATES

State	Pilot High	Pilot Low	Frequency	EV Resistance	Description
STATE A	+12V	N/A	DC	N/A	Not Connected
STATE B	+9V	-12V	1 kHz	2.74k	EV Connected (Ready)
STATE C	+6V	-12V	1 kHz	882	EV Charge
STATE D	+3V	-12V	1 kHz	246	EV Charge (Vent. Required)
STATE E	0V	0V	N/A		Error
STATE F	N/A	-12V	N/A		Unknown/Error

<sup>&</sup>lt;sup>1</sup>A solution to this problem is to connect a high power vehicle-to-load (V2L) bidirectional converter to discharge the EV battery to an external load via the available communication standard, but we did not have the V2L hardware available at the laboratory at the time of this study.

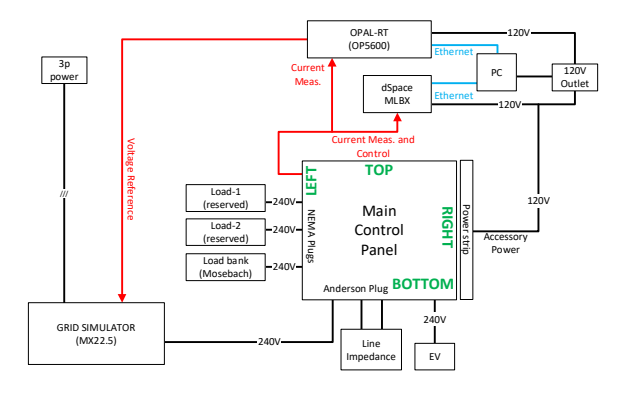


Fig. 2. High level system integration.

due to the loading of the EV connector, and this is captured by reading-in this signal through one of the ANALOG-IN channels of MLBX.

Besides the low-level charging protocol, a higher-level charging control algorithm is also implemented on MLBX, thanks to its high computing capability. The charging algorithm also makes use of real-time voltage and charging current as feedback. Therefore, charging voltage and current are sensed and fed back to MLBX through its ANALOG-IN channels. The overall EVSE controller software was designed in MATLAB/Simulink, compiled for MLBX, and operated at 1 kHz.

### D. Power and Control Panel Design

The physical integration schematics of the system described in Fig. 1 is shown in Fig. 2. An electrical power and control panel is designed to electrically isolate, organize, and house the physical coupling points of the EVGI test-bed. The hardware picture of the panel is shown in Fig. 3. The panel was designed to distribute the main AC power from the grid simulator to four different loads (including the EV) via individual 50 A circuit breakers. All the loads are connected through the line impedance housed in a separate panel. The main circuit breaker in the control panel can be tripped by an emergency button installed on the panel for emergency shutdown of the system. The measured voltage and current signals are processed through signal conditioning circuits and sent to the RTS and MLBX. The custom EVSE circuit is also located near the EV power connection point in the control panel. This circuit controls a relay to switch on/off EV charging. The low-power circuitry inside the panel is powered by a 24 V, 30 W power supply.

### E. Hardware Integration

The proposed EVGI test-bed is integrated as shown in Fig. 4. The charging process was controlled through a software interface designed in dSPACE ControlDesk. The control PC communicates with dSPACE and OPAL-RT in real-time to monitor the grid model and the EVSE status. The J1772 standard controls the charging current according to (1). It should be noted that the minimum EV charging current is set to

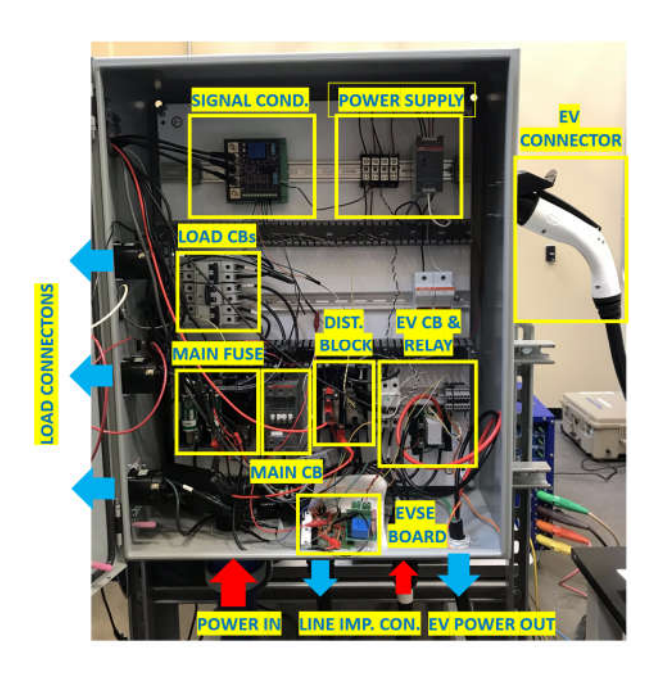
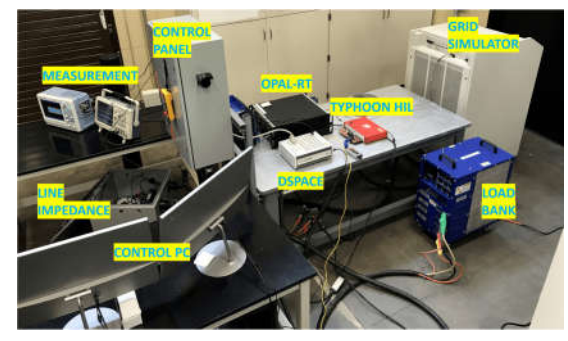


Fig. 3. Detailed hardware picture for the main power and control panel.



(a) HIL test-bed (front view).

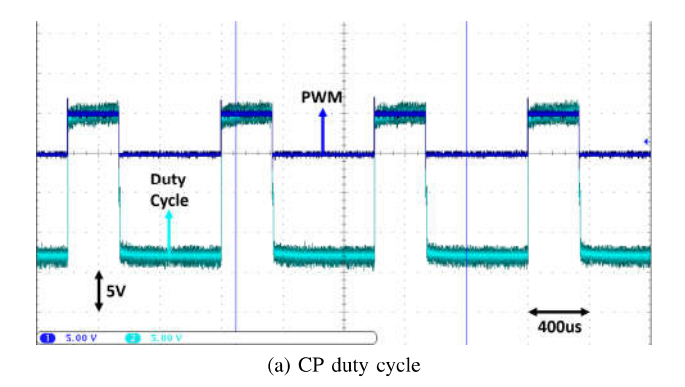


(b) HIL test-bed (side view).

Fig. 4. HIL test-bed integration.

7 A during all hardware tests to get a good converter response. This is just 1 A above the standard's minimum allowable charging current.

Fig. 5a shows the PWM signal in blue (generated by dSpace) and the CP duty cycle signal in cyan (generated by the custom EVSE board). The high side of the CP represents the EV state. The waveform in Fig. 5a was obtained for  $I_{EV}$ =20A



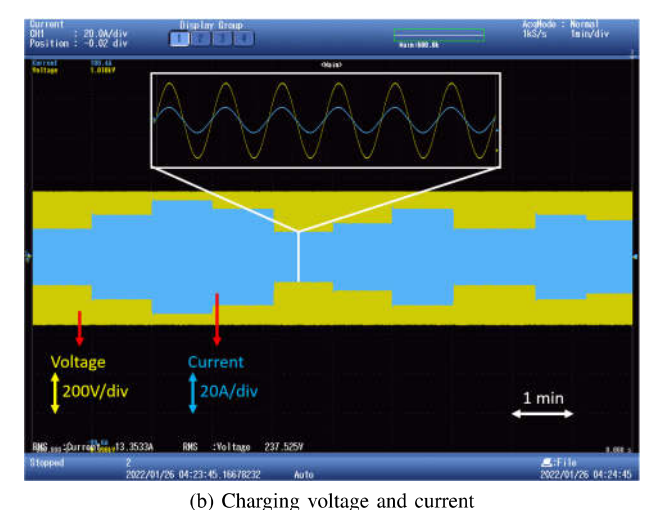


Fig. 5. 10 min test charging session waveforms

with d=33.3%. The EV charging voltage and current were probed by a YOKOGAWA DL850E DAQ device and shown in Fig. 5b for a test charging session of  $10 \, \text{min}$ . Also, a six grid-cycle zoomed version of the current/voltage waveform is included. For the test session, the EV charging current is regulated at different current levels via the custom-designed EVSE.

## III. SCALABLE, DECENTRALIZED, SMART CHARGING MANAGEMENT

### A. AIMD-based EV Charging Algorithm

In order to test the designed EVGI HIL test-bed, we developed a scalable, decentralized, smart charging algorithm based on the Additive Increase and Multiplicative Decrease (AIMD) algorithm [26], [27]. The proposed smart charging algorithm aims to detect and reduce the power grid congestion caused by mass EV penetration. The algorithm uses the local end-node voltage to predict the power congestion level of the distribution grid using a linear model. In the context of this study, the power congestion refers to the total three-phase apparent power (S) of the substation transformer that powers the downstream network. This model is trained for each end-node by using the historical end-node voltage and total substation power measurements. The training data were generated by a running a 30-day computer simulation of an

### Algorithm 1 AIMD algorithm for EV charging network

```
Input: Substation preset congestion level: PCL
Compute: [\theta_0, \theta_1] based on historical V_i and S measurements
Parameter: AI parameter: \alpha_i > 0
Parameter: MD parameter: 0 < \beta_i < 1
Parameter: Voltage update period: T_u
Parameter: Algorithm action period: T_a
Input: Previous charging current: I_i(t)
Output: New charging current: I_i(t+1)
 1: for t \in \{0, 1, \dots, T\} do
         for t \in \{0, T_u, 2T_u, \cdots, kT_u\} do
 2:
 3:
              \overline{V_i} \leftarrow \text{EWMA}(V_i(t))
              for t \in \{0, T_a, 2T_a, \cdots, kT_a\} do S^p(t) \leftarrow \theta_0 + \theta_1 \overline{V_i}
 4:
 5:
                  if S^p(t) < PCL and V_i^{en} > V_{min} then
 6:
                       I_i(t+1) \leftarrow I_i(t) + \alpha_i
 7:
 8:
 9:
                       I_i(t+1) \leftarrow \beta_i \times I_i(t)
                   end if
10:
              end for
11:
         end for
12:
13: end for
```

equivalent phasor simulation of the real-time grid model to save time and effort. The training is performed using linear regression (LR). After the training, each end-node is assigned a linear model with two coefficients  $[\theta_0, \theta_1]$  that maps their voltage measurements  $(V_i)$  to a predicted substation power  $(S^p)$  value:

$$S^p(t) = \theta_0 + \theta_1 V_i(t). \tag{2}$$

An exponentially weighted moving average (EWMA) filter can also be used to filter out some local dynamics from the voltage measurements. By predicting the total substation power  $(S^p(t))$  using local voltage measurements, end-nodes can autonomously determine whether there is congestion in the grid by comparing  $S^p$  with a pre-set congestion level (PCL) set by the grid network operator. PCL could be the substation rated power or some lower level beyond which the grid is said to be congested. Algorithm 1 is proposed as an adaptation of AIMD for EV charging control.

The additive increase (AI) and multiplicative decrease (MD) parameters  $(\alpha_i \text{ and } \beta_i)$  can be chosen based on the grid dynamics and EV charging characteristics. Depending on the computational limitations, the sampling period of the voltage could be adjusted by the parameter  $T_u$ . The algorithm action period  $(T_a)$  determines how often AIMD performs congestion check and takes action. Choosing  $T_a$  again depends on the grid and the on-board EV charger dynamics. At every  $T_a$  interval, the substation total power demand is predicted using (2). If the predicted value  $S^p$  is less than PCL, and the end-node voltage  $(V_i^{en})$  is higher than the minimum service voltage  $(V_{min})$ , the congestion level is likely not reached, and there is still capacity in the system. Hence, the EV charging current is additively increased by  $\alpha_i > 0$ . If this condition does not

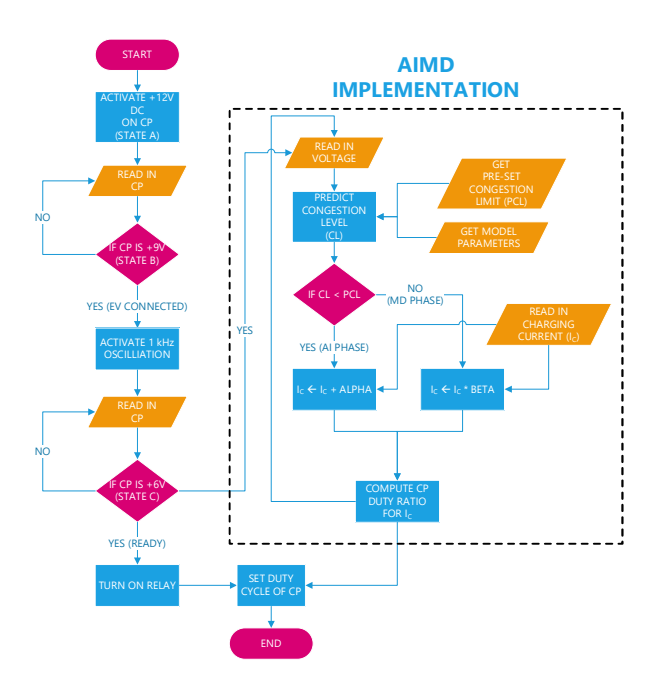


Fig. 6. Flow chart of the EVSE.

hold, the algorithm's MD phase steps in and scales down the charging current by  $0 < \beta_i < 1$ . The flow chart of the charging algorithm and EVSE level control is shown in Fig. 6. More information on the operation of the AIMD algorithm can be found in the previous studies of the authors [27]–[30].

### B. Performance Evaluation

From a demand-side management perspective, an EV charging control algorithm should avoid overloading the grid infrastructure (e.g., substation transformer and distribution lines), utilize the available capacity, and satisfy EV customer expectations as much as possible. In this regard, three performance metrics are developed to measure the effectiveness of the presented charging algorithm.

1) Maximum loading percentage (MLP): MLP is defined as the ratio of the maximum substation apparent power in pu to the pre-set congestion level (PCL). PCL could be the transformer's rated power as well as a lower set point determined by the system operator.

$$MLP = \frac{max(S(t))}{\text{Pre-set congestion level (PCL)}} \times 100\%, \quad (3)$$

where t is the simulation time, and S(t) is the substation total apparent power resulted from the implementation of the charging algorithm.

2) Capacity utilization (CU): CU is defined as the percent ratio of the grid capacity (in terms of energy) utilized as a result of implementing a charging algorithm to the capacity that could have been used in the case of an ideal AIMD implementation. The ideal AIMD refers to the fictitious case where the end-nodes are notified of the true grid congestion signal. Therefore, the CU score of the ideal AIMD algorithm would be 100% by default as it can use all the available

capacity thanks to the actual congestion feedback. CU is defined as follows:

$$CU = \frac{\int_{t_1}^{t_2} (S(t) - S^{base}(t)) dt}{\int_{t_1}^{t_2} (PCL - S^{base}(t)) dt} \times 100\%, \tag{4}$$

where  $t_1$  and  $t_2$  are the start and end times during which the ideal AIMD algorithm uses up the full capacity determined by PCL.  $S^{base}(t)$  is the baseload of the grid after the EV load is removed.

3) Average charging power (ACP): ACP is the average charging power of the vehicle for a given time interval.

### IV. HIL SIMULATION CASE STUDIES

The proposed AIMD-based EV charging control algorithm using the end-node voltage was tested on the HIL test-bed shown in Fig. 4. Two case studies (Case-I and Case-II) are developed to evaluate the algorithm's performance. Both cases are simulated for one hour on the test distribution grid described in Fig. 1.

Case-I investigates the responsiveness of the proposed algorithm in case of a significant load increase. For this case, PCL was set to 0.7 pu in the AIMD operation, and the system loads were increased between 750 s and 2250 s. The goal is to control the system congestion level around PCL during EV charging. However, the increase of the uncontrolled system loads increases the system peak power up to around the same level as PCL (0.7 pu). The EVs should detect the load increase and reduce their charging power during this time in a decentralized way. This case has three-time intervals. The first interval  $(t < 750 \, \text{s})$  covers the arrival time of EVs. The second interval  $(750 \, \text{s} \le t \le 2250 \, \text{s})$  is when the system loads gradually increase, stay stable for some time and decrease again. The third interval  $(t > 2250 \, \text{s})$  goes back to the expected level of the system loads.

Case-II tests the ability of the algorithms to operate at different PCL. The simulation time is split into three intervals. The first interval ( $t < 1000 \, \mathrm{s}$ ) implements uncontrolled charging where all EVs are charged at the rated current of 27 A. The second interval ( $1000 \, \mathrm{s} \! \leq \! t \! < \! 2500 \, \mathrm{s}$ ) switches to the AIMD control with a PCL of 0.7 pu. The transition between the first two intervals also shows the difference between uncontrolled and controlled EV charging. The third interval ( $2500 \, \mathrm{s} \! \leq \! t \! \leq \! 3600 \, \mathrm{s}$ ) changes PCL to 0.8 pu by allocating higher capacity for charging. The transition between the second and third intervals demonstrates how the end-nodes detect the capacity increase and respond by increasing their average charging power.

The AI and MD parameters of the AIMD algorithms are set to 1 and 0.5, respectively. The voltage update period  $(T_u)$  is set to 1 s. The algorithm period  $(T_a)$  is set to 15 s to better observe AIMD actions within the one-hour simulation duration.

1) Case-I: Load increase: Fig. 7 demonstrates the end-node pu voltage, EV charging current, and actual and predicted total substation power  $(S \text{ and } S^p)$  in pu. The green dotted lines mark the starting and ending of the three time intervals. The

MLP and CU scores and the average charging power of Nissan Leaf in the three intervals are given in Table II.

MLP stays below 100% (0.7 pu) in the first and third intervals, indicating that the AIMD charging effectively holds the grid congestion below PCL. ACP is around 2.14kW in the first interval. The second interval is dominated by the uncontrolled loads increasing MLP up to 100%. The increase of the system loads decreases the end-node voltage and causes AIMD to go into the MD phase more often. This overall results in a reduced ACP of 1.60 kW. After the system loads return to the normal level at the beginning of the third interval, the system capacity increases, yielding an ACP of 2.04kW, similar to the first interval. The CU scores are above 75% for the first and third intervals but slightly below 70% for the second interval due to the increased system loads. This node's predicted substation power  $(S^p)$  is slightly above the actual substation power (S), especially for the first and third intervals lowering the potential CU score. It triggers the MD phase of the AIMD algorithm at the points where  $S^p$  hits the PCL line. In the second interval, the end-node voltage is significantly reduced by the increased uncontrolled system loads and local consumption resulting in over-prediction and reduced average charging power.

2) Case-II: Different congestion levels: This case study first compares uncontrolled charging with the AIMD control. Fig. 8 shows the end-node voltage, EV charging current, and actual and predicted substation total power. The first interval in Case-II simulates uncontrolled charging. During this interval, the EV charging current is set to its maximum (27 A), yielding an average charging power of 6.23 kW (Table III). Note that the voltage in this interval significantly drops due to the heavy system congestion. The uncontrolled charging results in a highly congested grid with an MLP of 134.54%.

In the second interval, the EVs start implementing the AIMD charging control with a PCL of 0.7 pu. As a result,

TABLE II PERFORMANCE SCORES OF CASE-I

Time interval	MLP (%)	CU (%)	ACP of Nissan Leaf (kW)
t < 750s	91.08	75.35	2.14
$750s \le t < 2250s$	100	69.38	1.60
$2250s \le t \le 3600s$	93.30	77.66	2.04

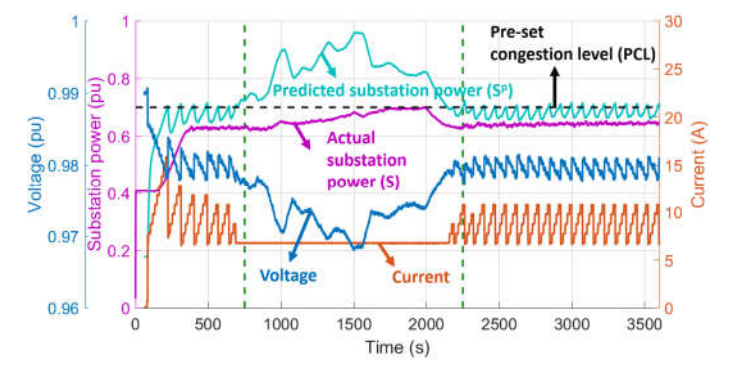


Fig. 7. RMS EV current and voltage, and actual and predicted substation power for Case-I.

### TABLE III PERFORMANCE SCORES OF CASE-II

Time interval	MLP (%)	CU (%)	ACP of Nissan Leaf (kW)
t < 1000s	134.54	N/A	6.23
$1000s \le t < 2500s$	92.35	77.61	1.92
$2500s \le t \le 3600s$	91.68	78.16	2.39

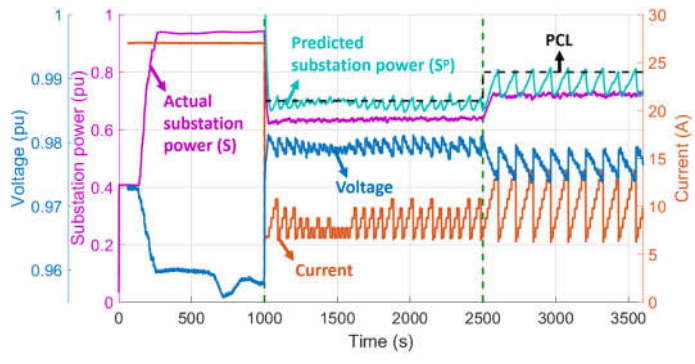


Fig. 8. RMS EV current and voltage, and actual and predicted substation power for Case-II.

MLP drops below 100% for this interval with a CU score of 77.61%. S goes below PCL and stays fairly constant during the second interval showing that the system's congestion is controlled under PCL. As a result, the EV's average charging power drops from  $6.23\,\mathrm{kW}$  to  $1.92\,\mathrm{kW}$ .

At the second transition (t=2500 s), PCL changes to 0.8 pu for all EVs. The EV quickly responds to the capacity increase by increasing its average charging power to 2.39 kW. The transient capacity increase did not make the system unstable. S gradually increased and sat on a higher level slightly lower than the PCL resulting in an MLP of 91.68% and CU of 78.16%.  $S^p$  is again slightly over the actual S causing the grid to sit on a congestion level lower than PCL. This is mainly because the end-node voltage is sensitive to local dynamics, affecting the prediction results.

### V. Conclusions

An EVGI hardware test-bed is an essential step prior to deploying a smart charging algorithms out on the field. It provides valuable and cost effective insights into possible outcomes and hardware/software challenges of EV integration. The grid-related challenges can also be emulated and addressed in real time by creating virtual events (i.e., faults, service interruptions, etc.) in the RTS triggered by real loads. This platform also supports the integration and testing of any power electronics based loads and sources (i.e., ESS, PV inverters, motor drives, etc.) under different scenarios. To this end, this study presents a detailed guideline for designing and operating an EVGI hardware test-bed. The test-bed components, and their roles and interactions within the system are described.

This work also presented a HIL implementation of an AIMD based smart EV charging control algorithm on the designed hardware test-bed. The charging algorithm was implemented based on the J1772 standard using a custom EVSE running on a dSpace MicroLabBox platform. The results showed that

the AIMD algorithm successfully detected and eliminated the grid congestion.

### REFERENCES

- [1] K. Qian, C. Zhou, and Y. Yuan, "Impacts of high penetration level of fully electric vehicles charging loads on the thermal ageing of power transformers," *Int. J. Electr. Power Energy Syst.*, vol. 65, pp. 102–112, 2015. [Online]. Available: https://www.sciencedirect.com/science/article/pii/S0142061514005912
- [2] S. A. A. Rizvi, A. Xin, A. Masood, S. Iqbal, M. U. Jan, and H. Rehman, "Electric vehicles and their impacts on integration into power grid: A review," in *IEEE Conf. Energy Internet and Energy Syst. Integr. (E12)*, 2018, pp. 1–6.
- [3] F. Erden, M. C. Kisacikoglu, and O. H. Gurec, "Examination of EV-grid integration using real driving and transformer loading data," in *Int. Conf. Elect. Electron. Eng.*, 2015, pp. 364–368.
- [4] L. P. Fernandez, T. G. S. Roman, R. Cossent, C. M. Domingo, and P. Frias, "Assessment of the impact of plug-in electric vehicles on distribution networks," *IEEE Trans. Power Syst.*, vol. 26, no. 1, pp. 206– 213, Feb. 2011.
- [5] S. Shafiee, M. Fotuhi-Firuzabad, and M. Rastegar, "Investigating the impacts of plug-in hybrid electric vehicles on power distribution systems," *IEEE Trans. Smart Grid*, vol. 4, no. 3, pp. 1351–1360, 2013.
- [6] E. Veldman and R. A. Verzijlbergh, "Distribution grid impacts of smart electric vehicle charging from different perspectives," *IEEE Trans. Smart Grid*, vol. 6, no. 1, pp. 333–342, 2015.
- [7] N. Leemput, F. Geth, J. Van Roy, A. Delnooz, J. Buscher, and J. Driesen, "Impact of electric vehicle on-board single-phase charging strategies on a flemish residential grid," *IEEE Trans. Smart Grid*, vol. 5, no. 4, pp. 1815–1822, 2014.
- [8] H. Nazir, "Lessons learned from the february 2021 texas power outage," CERI Electricity Report, 2021.
- [9] M. Leslie, "Texas crisis highlights grid vulnerabilities," 2021.
- [10] D. Wu, X. Zheng, Y. Xu, D. Olsen, B. Xia, C. Singh, and L. Xie, "An open-source model for simulation and corrective measure assessment of the 2021 texas power outage," arXiv preprint arXiv:2104.04146, 2021.
- [11] E. Ucer, N. Erdogan, S. Rahman, and M. C. Kisacikoglu, "Real-time simulation of ev grid integration with internet-inspired charging control," in 3rd E-Mobility Power System Integration Symposium, 2019.
- [12] V. Lakshminarayanan, G. Selvaraj, K. Rajashekara, L. Ben-Brahim, and A. Gastli, "Hardware in loop (hil) testing of energy management controller for electric vehicle integrated microgrid," in 2019 North American Power Symposium (NAPS), 2019, pp. 1–6.
- [13] V. Lakshminarayanan, V. G. S. Chemudupati, S. K. Pramanick, and K. Rajashekara, "Real-time optimal energy management controller for electric vehicle integration in workplace microgrid," *IEEE Transactions* on *Transportation Electrification*, vol. 5, no. 1, pp. 174–185, 2019.
- [14] J. Zelic, L. Novakovic, İ. Klindo, and G. Gruosso, "Hardware in the loop framework for analysis of impact of electrical vehicle charging devices on distribution network," in *IEEE Vehicle Power and Propulsion Conference (VPPC)*, 2020, pp. 1–5.
- [15] I. Jayawardana, C. N. M. Ho, and Y. Zhang, "A comprehensive study and validation of a power-hil testbed for evaluating grid-connected ev chargers," *IEEE Journal of Emerging and Selected Topics in Power Electronics*, pp. 1–1, 2021.
- [16] B. P. Bhattarai, M. Lévesque, M. Maier, B. Bak-Jensen, and J. Radhakrishna Pillai, "Optimizing electric vehicle coordination over a heterogeneous mesh network in a scaled-down smart grid testbed," *IEEE Trans. Smart Grid*, vol. 6, no. 2, pp. 784–794, 2015.
- [17] F. Marra, D. Sacchetti, A. B. Pedersen, P. B. Andersen, C. Træholt, and E. Larsen, "Implementation of an electric vehicle test bed controlled by a virtual power plant for contributing to regulating power reserves," in IEEE Power Energy Soc. General Meeting, 2012, pp. 1–7.
- [18] C. Flack, E. Ucer, C. P. Smith, and M. Kisacikoglu, "Controller hardware-in-the-loop (c-hil) testing of decentralized ev-grid integration," 2022. [Online]. Available: https://arxiv.org/abs/2205.00460
- [19] A. R. Malekpour and A. Pahwa, "Radial test feeder including primary and secondary distribution network," in *North American Power Symp.*, Oct. 2015, pp. 1–9.
- [20] E. Ucer, S. Rahman, A. McDonald, and M. Kisacikoglu. (2019) Residential active/reactive power consumption, voltage, and frequency data for a house in Alabama. [Dataset] https://ir.ua.edu/handle/123456789/6346. [Online; accessed 15-Jul-2020].

- [21] Energy monitoring systems for residential and commercial applications. http://www.egauge.net/. [Online; accessed 6-Jun-2022].
- [22] E. Ucer, M. Kisacikoglu, A. Gurbuz, S. Rahman, and M. Yuksel, "A machine learning approach for understanding power distribution system congestion," in *IEEE Energy Convers. Congr. and Expo. (ECCE)*, 2020, pp. 1977–1983.
- [23] B. Ahmed, A. Abdelgadir, N. A. Saied, and A. A. Karrar, "A compensated distributed-parameter line decoupling approach for real time applications," *IEEE Trans. Smart Grid*, vol. 12, no. 2, pp. 1761–1771, 2021.
- [24] C. Dufour, J. Mahseredjian, and J. Belanger, "A combined state-space nodal method for the simulation of power system transients," in *IEEE Power Energy Soc. General Meeting*, 2011, pp. 1–1.
- [25] SAE j1772: Electric Vehicle and Plug in Hybrid Electric Vehicle Conductive Charge Coupler. http://standards.sae.org/j1772\_201001.
- [26] D. M. Chiu and R. Jain, "Analysis of the increase/decrease algorithms for congestion avoidance in computer networks," *Journal of Computer Networks and ISDN Systems*, vol. 17, no. 1, pp. 1–14, June 1989.
- [27] E. Ucer, M. C. Kisacikoglu, M. Yuksel, and A. C. Gurbuz, "An internet-inspired proportional fair EV charging control method," *IEEE Syst. J.*, vol. 13, no. 4, pp. 4292–4302, Dec. 2019.
- [28] E. Ucer, M. C. Kisacikoglu, and M. Yuksel, "Analysis of an Internetinspired EV charging network in a distribution grid," in *IEEE/PES Transmiss. Distr. Conf.*, April 2018, pp. 1–5.
- [29] E. Ucer, M. C. Kisacikoglu, and A. C. Gurbuz, "Learning EV integration impact on a low voltage distribution grid," in *IEEE Power Energy Soc. General Meeting*, Aug. 2018, pp. 1–5.
- [30] E. Ucer, M. C. Kisacikoglu, and M.Yuksel, "Analysis of decentralized AIMD-based EV charging control," in *IEEE Power Energy Soc. General Meeting*, Aug 2019, pp. 1–5.